Computer Modeling in Engineering & Sciences

Tech Science Press

DOI: 10.32604/cmes.2023.022155

check for updates

ARTICLE

Numerical Simulation Analysis of the Transformer Fire Extinguishing Process with a High-Pressure Water Mist System under Different Conditions

Haowei Yao[1,3,*], Youxin Li[1,3], Kefeng Lv[1,3], Dong Wang[2,3], Jinguang Zhang[4], Zhenyu Zhan[2,3], Zhenyu Wang[2,3], Huaitao Song[1,3], Xiaoge Wei[1,3] and Hengjie Qin[1,3]

[1]College of Building Environment Engineering, Zhengzhou University of Light Industry, Zhengzhou, 450001, China

[2]Electric Power Research Institute, State Grid Henan Electric Power Company, Zhengzhou, 450052, China

[3]Zhengzhou Key Laboratory of Electric Power Fire Safety, Zhengzhou, 450001, China

[4]State Grid Henan Electric Power Corporation Maintenance Company, Zhengzhou, 450052, China

*Corresponding Author: Haowei Yao. Email: yaohaowei@zzuli.edu.cn

Received: 21 May 2022 Accepted: 05 September 2022

ABSTRACT

To thoroughly study the extinguishing effect of a high-pressure water mist fire extinguishing system when a transformer fire occurs, a 3D experimental model of a transformer is established in this work by employing Fire Dynamics Simulator (FDS) software. More specifically, by setting different parameters, the process of the high-pressure water mist fire extinguishing system with the presence of both diverse ambient temperatures and water mist sprinkler laying conditions is simulated. In addition, the fire extinguishing effect of the employed high-pressure water mist system with the implementation of different strategies is systematically analyzed. The extracted results show that a fire source farther away from the centerline leads to a lower local temperature distribution. In addition, as the ambient temperature increases, the temperature above the fire source decreases, while the temperature and the concentration of the upper flue gas layer both decrease. Interestingly, after the high-pressure water mist sprinkler begins to operate, both the temperature distribution above the fire source and the concentration of the flue gas decrease, which indicates that the high-pressure water mist system plays the role of cooling and dust removal. By comparing various sprinkler laying methods, it is found that the lower sprinkler height has a better effect on the temperature above the fire source, the temperature of the upper flue gas layer, and the concentration of the flue gas. Moreover, when the sprinkler is spread over the whole transformer, the cooling effect on both the temperature above the fire source and the temperature of the upper flue gas layer is good, whereas the change in the concentration of the flue gas above the fire source is not obvious compared to the case where the sprinkler is not fully spread.

KEYWORDS

Transformer fire; high-pressure water mist; temperature; flue gas concentration

1 Introduction

With the constant development of science and technology, the construction process of ultra-high voltage power grids is accelerating, whereas the number of large transformers is also increasing [1–3]. However, while people's living standards are improving, the demand for electricity consumption is also increasing, and transformers are entering an overloaded state that is prone to failures [4], the most important type of which is power failure without a specific reason. Since a transformer contains a large amount of transformer oil, the transformer oil combustion procedure is a high-strength turbulent combustion phenomenon, including a large amount of complex physical and chemical effects. Overall, this procedure can be divided into the initial growth stage and the full combustion and weakening stages [5]. A failure event may cause a transformer to malfunction and cause damage to the electrical equipment, whereas a fire may potentially affect the safe and stable operation of the power grid and even impact the safety of society [6–10]. Therefore, the safety of a transformer has become a very important issue that has to be addressed.

A transformer fire is categorized as an electrical fire, and electrical equipment is an important part of the fire load in buildings [11]. Compared with an ordinary fire, it is more difficult to extinguish an electrical fire, since this requires a fire extinguishing medium with both high isolation performance and fire extinguishing efficiency [12]. Along these lines, high-pressure water mist is a fire extinguishing system that works by isolating oxygen molecules and cooling down the temperature [13]. Additionally, through a sprinkler, the system can spray fine water mist at a specific pressure to extinguish a fire. It should be emphasized that for the same volume, the water droplets of the high-pressure water mist are small, with high density and a large dispersion area, which both play a crucial role in the cooling effect. The high-pressure water mist can also form a protective zone around the fire source, in terms of cooling and blocking oxygen, and as a result, it can quickly extinguish the fire. Furthermore, high-pressure water mist has good insulation for electrical equipment [14,15]. Therefore, the fire extinguishing capabilities of a high-pressure water mist fire extinguishing system are much higher than those of conventional water sprinkler fire extinguishing systems that are often used to put out transformer fires and other accidents.

Chen et al. [16] analyzed the impact of pressure on the characteristics of a fine mist field using the computational hydrodynamic software program Fluent. They found that most water mist particles were under the sprinkler. The farther the horizontal distance was from the nozzle, the lower the number of mist particles was. Moreover, Yang et al. [17] analyzed the fire extinguishing effects of a single sprinkler and four-sprinkler fine water mist with the enforcement of different spray pressures. They revealed that the spray pressure had a great influence on the properties of a single sprinkler. Ma et al. [18] studied the working mechanism of high-pressure water mist on fire extinguishing for a gasoline pool with the application of different injection modes. The authors compared the characteristics of both continuous and pulse water mist spraying to extinguish an oil pool fire. They found that pulse-type spraying could extinguish an oil pool fire more effectively since the pulse-type spraying exhibited a high cooling rate. In another interesting research project, Chan et al. [19] studied the spray characteristics of a two-fluid sprinkler configuration on water mist and the heptane pool fire extinguishing performance. Gong et al. [20] conducted a fire extinguishing experiment for a multi-sprinkler combined with high-pressure water mist sprinklers. They compared and analyzed the fire extinguishing effects by employing different sprinkler pressures, heights, and quantities. Lu et al. [21] found that an additive significantly improved the fire extinguishing performance of water mist. In addition, Wang et al. [22] simulated and analyzed the fire extinguishing efficiency of a high-pressure water mist fire extinguishing system with the employment of different injection speeds and pressures with FDS and other technologies. The authors demonstrated that when the injection speed and

pressure characteristics increased by a certain value, the cooling and fire source control effects were better. Chen et al. [23] carried out a live insulation experiment for a transformer, and they found that the insulation capacity of the fine water mist exhibited a good insulation ability. Furthermore, Zhang et al. [24] used FDS to simulate a comprehensive pipe gallery with openings at both ends, and studied the influence of the sprinkler arrangement on the fire extinguishing effect. The authors found that when the sprinklers were arranged vertically, the fire extinguishing effect at an interval of 3 m was higher than that at an interval of 2 m. Wang et al. [25] investigated the dust removal effect of different spray pressure loads on coal dust. The authors divulged that an elevated spray pressure led to an improved dust removal effect. However, no significant improvement was recorded when the spray pressure exceeded the value of 10 MPa. Additionally, Sun et al. [26] studied the axial temperature distribution of a transformer oil injection fire plume by changing the heat source. They disclosed that the local temperature distribution increased as the heat release rate of the heat source became bigger. Yuan et al. [27] compared the inhibitory effect of water mist on a hydrogen jet fire with the utilization of different droplet sizes, spray speeds, and environmental wind speeds. The authors found that the selection of appropriate parameters was conducive to reducing the temperature on the fire site and inhibiting further development of the fire.

With this perspective, the main goal of this work is to explore studies of the influence of high-pressure water mist on the extinguishing of a transformer fire by taking into account different conditions. More specifically, by performing comprehensive numerical simulations [28,29], the impacts of different ambient temperature distributions and high-pressure water mist fire extinguishing techniques with the application of various sprinkler laying strategies are systematically analyzed. It should be emphasized that the temperature profiles above the fire source and the flue gas layer as well as the concentration of the flue gas are thoroughly investigated. Our work provides fruitful theoretical insights for the development of a high-pressure water mist fire extinguishing system with enhanced properties.

2 Model Setting and Method

2.1 The Solution Formula of FDS

When simulating fire with FDS software, the mixed component combustion model can satisfy the research on the thermal effect of the flame. Its general chemical reaction formula is:

$$v_F\left(C_xH_yO_z\right)+v_{o_2}\rightarrow\sum_t v_p\,(\mathrm{Pro}ducts) \tag{1}$$

To analyze data such as flue gas concentration in the combustion process, a finite chemical reaction rate model is used for the calculation. Its general chemical reaction formula is [30]:

$$v_{C_xH_y}\left(C_xH_y\right)+v_{O_2}\left(O_2\right)\rightarrow v_{CO_2}\left(CO_2\right)+v_{H_2O}\left(H_2O\right) \tag{2}$$

Its chemical reaction rate is:

$$\frac{d\left(C_xH_y\right)}{dt}=-A\left(C_xH_y\right)^a\left(O_2\right)^b e^{-\frac{E}{RT}} \tag{3}$$

In the formula, A is the activation energy reaction pre-exponential factor; v is the chemical reaction coefficient; E is the activation energy of the reaction, J/mol; R is the molar gas constant, taking 8.314 J/(mol · K); T is the thermodynamic temperature, K; a and b are the reaction coefficients.

The cumulative volume distribution of the liquid spray ejected from the nozzle in FDS software can be represented by a combination of log-normal and Rosin-Rammler distribution functions [31]:

$$F(D) = \begin{cases} \dfrac{1}{\sqrt{2\pi}} \int_0^D \dfrac{1}{\sigma D'} e^{-\frac{\left[\ln\left(\frac{D'}{d_m}\right)\right]^2}{2\sigma^2}} dD' \ (d_m \geq D) \\ 1 - e^{-0.693\left(\frac{D}{d_m}\right)^{\gamma}} \ (d_m < D) \end{cases} \tag{4}$$

In the formula, D' is the drop diameter; D is the upper limit of droplet size interval; d_m is the average droplet diameter.

The movement of water droplets released after the nozzle is described as:

$$\frac{d(m_d u_d)}{dt} = m_d - \frac{1}{2}\rho C_d \pi r_d^2 (u_d - u) |u_d - u| \tag{5}$$

In the formula, m_d is the single water droplet mass, kg; C_d is the resistance coefficient of water droplets moving in gas; ρ is the density of water, kg/m^3; u_d is the water droplet velocity, m/s $\left(u_d = \dfrac{d_{x_d}}{d_t}\right)$; u is the air velocity; r_d is the water droplet radius, μm; x_d is the spatial position of water droplets in the airflow field at any time, m.

2.2 *Model Setting*

During the simulations, the selected transformer size is 4 m × 11.5 m × 5 m, the fire source size is 2 m × 1 m, and the fire source heat release rate per unit area is 4000 kW/m^2, as is schematically illustrated in Fig. 1. The sprinkler start time is 100 s, and the sprinkler flow rate and the speed are 10 L/min and 90 m/s, respectively, whereas the injection angle is between 30° and 80°.

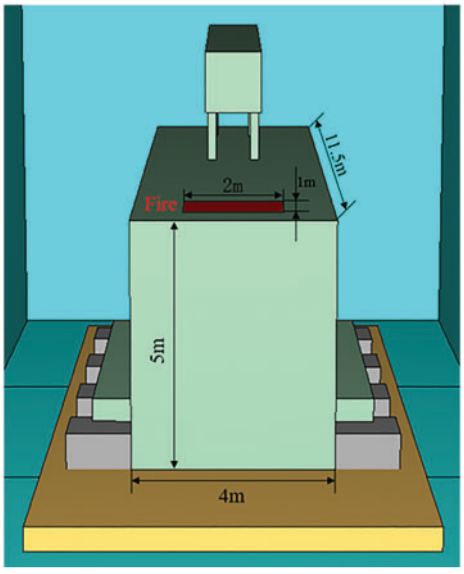

Figure 1: The employed transformer models

The thermocouple measuring point is set above the fire source, while the distances from the fire source are 0.75, 1.75, and 2.75 m. The temperature measurement point of the upper flue gas layer is set at a position 9.75 m above the fire source. The flue gas concentration measuring device is set at

a position 9.25 m above the fire source. The high-pressure water mist sprinkler is installed 9 m away from the ground, and the sprinkler spacing is 2.5 m. Two working conditions of the sprinklers being either full or not full are considered, as shown in Figs. 2a and 2b.

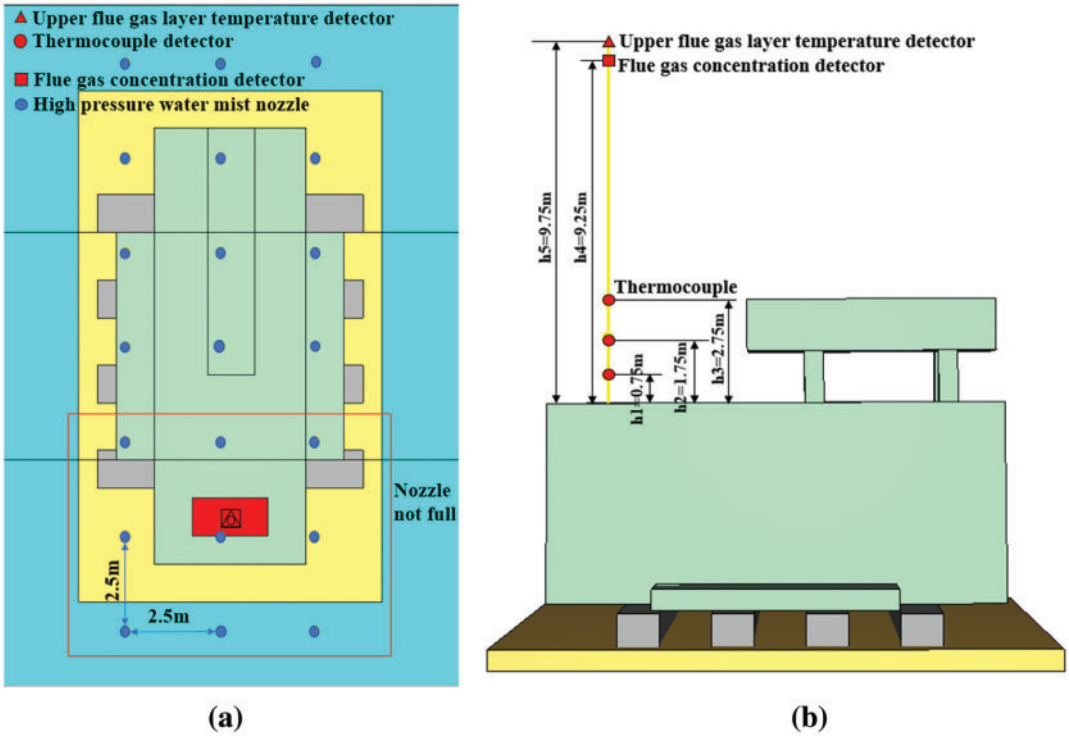

Figure 2: Detection points position: (a) Vertical view; (b) Side view

2.3 Working Condition Setting

During the simulation experiment, a total of three high-pressure water mist fire simulations with the enforcement of different conditions are set up. More specifically, working condition 1 is the simulation with the application of various ambient temperatures by comparing the relevant parameters at −10°C, −5°C, 0°C, 5°C, and 10°C. Moreover, working condition 2 is the simulation when the sprinklers are located at different heights and the sprinklers are compared. The relevant parameters in the two cases are explored when the distances from the ground are 9.5 and 9 m. As far as working condition 3 is concerned, a comparison of the parameters when the sprinkler is either covered with the top of the transformer or not covered is carried out. More details can be found in Table 1.

Table 1: Description of the working conditions

Working conditions	Instructions
working condition 1	Comparative analysis at different ambient temperatures (−10°C, −5°C, 0°C, 5°C, 10°C)

(Continued)

Table 1 (continued)

Working conditions	Instructions
working condition 2	Comparative analysis of sprinkler heads at different heights (9, 9.5 m)
working condition 3	Comparative analysis of full and not full sprinkler heads

2.4 Grid Independence Analysis

When performing numerical simulations, the selection of the proper grid density is believed to be of vital importance for the accuracy of the calculated outcomes. With respect to this, an elevated grid density leads to more accurate calculation results [32]. Generally, the ratio D^*/δ_x is used to express the accuracy of the fire source characteristic, where D^* is the characteristic diameter of the fire source, δ_x is the grid size, and the calculation formula of D^* is expressed as follows [33] (1):

$$D^* = \left(\frac{Q}{\rho_0 C_P \sqrt{g} T_0}\right)^{\frac{2}{5}} \tag{6}$$

where Q is the power of the fire source with units of kW, ρ_0 is the air density, which is assigned the value of 1.29 kg/m^3, C_P is the specific heat capacity of air, which generally takes the value of 1.005 kJ/(kg·K), g is the acceleration due to gravity, which generally takes the value 9.8 m/s^2, and T_0 is the ambient temperature that is ascribed the value of 273 K. Additionally, the fire source power in this simulation is set to the value of 8000 kW, which leads to a D^* value of about 2.21. It should be emphasized that when the dimensionless parameter value lies in the interval of 4–16, the acquired simulation calculation result is more accurate.

In the simulated framework, the flue gas concentrations when the grid sizes are 0.2, 0.25, and 0.33 are systematically compared. As can be seen from Fig. 3, when the grid size is 0.33, the fluctuation is large, and when the grid sizes are 0.2 and 0.25, both of the flue gas concentration change curves are relatively stable. When the problem of the simulation calculation time is considered, the grid size is set to 0.25 m × 0.25 m × 0.25 m in this simulation.

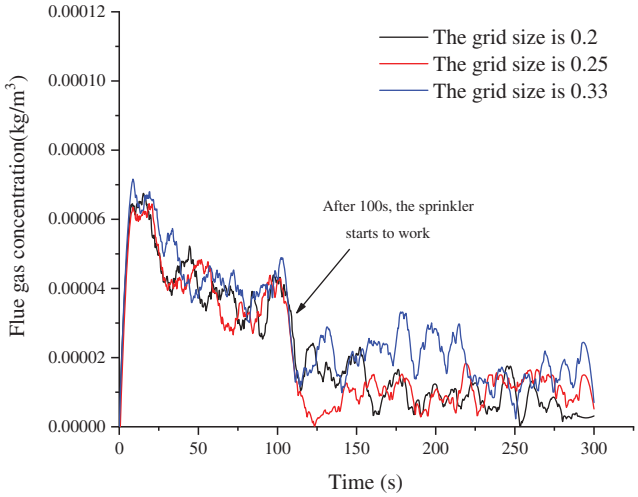

Figure 3: Comparison of the flue gas concentrations with the employment of different grid sizes

3 Analysis of the Simulated Results

3.1 Analysis of the Temperature Changes at Different Heights from the Fire Source

For the conditions of a sprinkler flow rate of 10 L/min, a flow speed of 90 m/s, and an ambient temperature of 10°C, the temperature distribution at different heights above the fire source is analyzed, and the following results are obtained:

As can be ascertained from Fig. 4, when the high-pressure water mist sprinkler is not working, the temperature above the fire source stabilizes in about 25 s. Furthermore, at different heights above the fire source (0.75, 1.75, and 2.75 m from the fire source), the average temperature changes (stable phase 1) are as follows: 446°C, 384°C, and 336°C. From the extracted outcomes, the conclusion can be drawn that the larger height above the fire source leads to a reduced temperature profile. After 100 s, the high-pressure water mist sprinkler starts to work, and the temperature above the fire source begins to decrease even more, while after 150 s, the temperature reaches a stable level. At this time, the average temperature variations above the fire source (stable phase 2) are 285°C, 192°C, and 145°C, which shows that the high-pressure water mist system does possess a cooling effect. The pattern of the decreasing temperature at different heights above the fire source is still maintained in this phase.

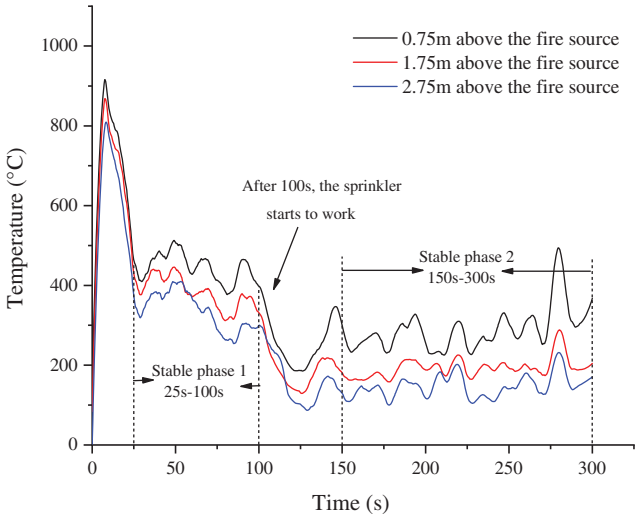

Figure 4: Distribution of the temperature changes at different heights above the fire source before and after spraying

3.2 Analysis of the High-Pressure Water Mist Fire Extinguishing Conditions for Different Ambient Temperatures

In a relatively low-temperature range (−10°C, −5°C, 0°C, 5°C, 10°C), the high-pressure water mist fire extinguishing system is thoroughly analyzed at different ambient temperatures, and the following results are obtained:

The dotted line that is illustrated in Fig. 5 represents the temperature change curve above the fire source. As can be seen from both Figs. 5 and 6, when the high-pressure water mist sprinkler is not working, the temperature above the fire source stabilizes at about 25 s, while for different ambient temperatures (−10°C, −5°C, 0°C, 5°C, and 10°C), the average temperature changes above the fire source (stable phase 1) are: 503°C, 471°C, 456°C, 448°C, and 446°C. Moreover, 100 s later, the high-pressure water mist sprinkler starts to work, and as a result, the temperature above the fire source

begins to decrease, while it is stabilized at about 150 s. At this time, the average temperature changes above the fire source (stable phase 2) are 371°C, 348°C, 343°C, 333°C, and 289°C, which indicates that the high-pressure water mist system plays a key role in the cooling down procedure. When the ambient temperature is low, the viscosity of the fuel increases, which leads to a slower combustion rate of the droplet and a larger movement path for the droplet, which increases the length of the flame [34,35], and the temperature above the fire source is relatively high. As the ambient temperature increases, the flame length decreases and the width increases, and the temperature above the fire source decreases as the flame height decreases. Therefore, the temperature profile above the ignition source decreases as the ambient temperature increases.

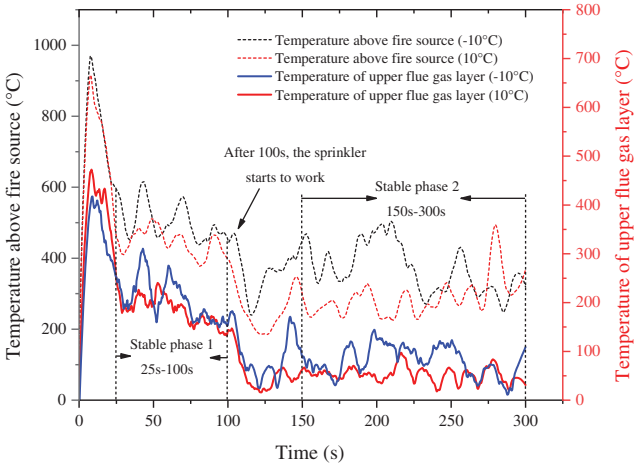

Figure 5: Temperature curves before and after the spraying process

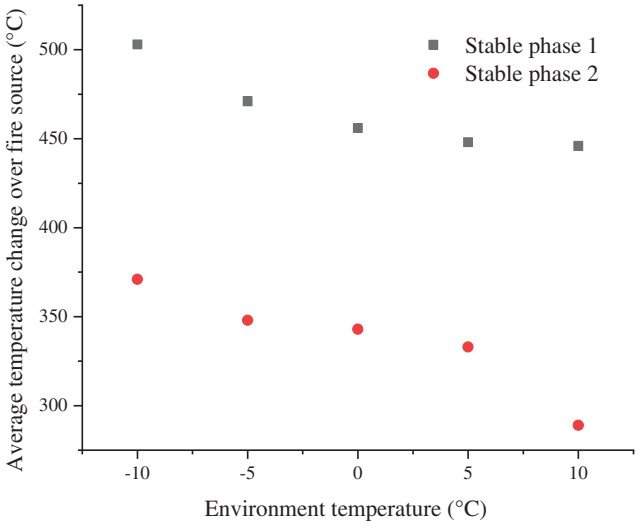

Figure 6: Comparison of the average temperature changes at different ambient temperatures

In addition, in Fig. 5, the solid line represents the temperature change curve of the upper flue gas layer. As can be ascertained from Figs. 5 and 7, when the high-pressure water mist sprinkler is not working, the temperature distribution of the upper flue gas layer stabilizes at about 25 s. It is interesting

to notice that with the application of different ambient temperature values (−10°C, −5°C, 0°C, 5°C, and 10°C), the average temperatures of the upper flue gas layer (stable phase 1) are 207°C, 200°C, 199°C, 177°C, and 184°C. In addition, it can be found that the temperature of the upper flue gas layer decreases when the ambient temperature rises. After 100 s, the high-pressure water mist sprinkler starts to work, and the temperature above the fire source begins to decrease. At this time, the average temperatures of the upper flue gas layer (stable phase 2) are 82°C, 35.1°C, 34.9°C, 41.4°C, and 52.8°C. Therefore, when the high-pressure water mist system is activated, it has a profound cooling effect on the upper flue gas layer.

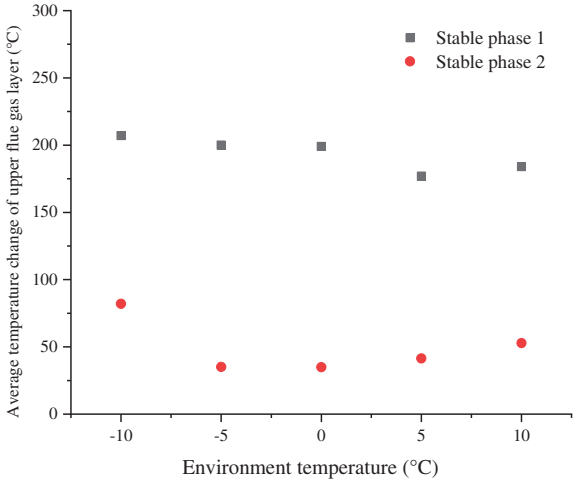

Figure 7: Temperature change curve of the upper flue gas layer for different ambient temperatures

After a transformer fire event occurs, when the high-pressure water mist system is not operating, the fire source reaches a stable state in about 25 s. Afterward, between 25 and 100 s, the average change of the flue gas concentration above the fire source at different ambient temperatures is shown in Table 2. From the overall change trend, with the increase in the ambient temperature, the flame burns completely. Therefore, the concentration of the flue gas shows a downward trend. After 100 s, the high-pressure water mist sprinkler starts to work and a stable state is attained at about 150 s. From Table 2, it can be clearly observed that when the high-pressure water mist system starts to work, the flue gas concentration decreases. Additionally, when the ambient temperature rises, the influence of the high-pressure water mist system fluctuates slightly, but the overall pattern shows a downward trend.

Table 2: Mean change of the flue gas concentration before and after the spraying process

Ambient temperature	25–100 s	After 150 s
−10°C	4.04×10^{-5} kg/m^3	2.13×10^{-5} kg/m^3
−5°C	3.63×10^{-5} kg/m^3	1.26×10^{-5} kg/m^3
0°C	3.82×10^{-5} kg/m^3	1.09×10^{-5} kg/m^3
5°C	3.41×10^{-5} kg/m^3	1.16×10^{-5} kg/m^3
10°C	3.61×10^{-5} kg/m^3	1.23×10^{-5} kg/m^3

3.3 Simulation for Different Sprinkler Layout Strategies

With the application of a high-pressure water mist with a flow rate of 10 L/min and a particle velocity of 80 m/s, through the deep analysis of the various data, the following results are obtained:

3.3.1 High-Pressure Water Mist Sprinklers at Different Heights

The dotted line in Fig. 8 represents the temperature change curve above the fire source. When the high-pressure water mist system is not working, the fire source reaches a stable state in about 25 s. In addition, at this time, the average temperature change above the fire source (stable phase 1) is 968°C. After the elapse of 100 s, the high-pressure water mist sprinkler begins to operate and the local temperature distribution above the fire source decreases, whereas the temperature above the fire source stabilizes at about 150 s. At this time, the calculated average temperature changes above the fire source for different sprinkler heights (9.0, 9.5 m) (stable phase 2) are 916°C and 927°C. Thus, it can be found that with the employment of the same initial conditions, the lower sprinkler height has a good cooling effect.

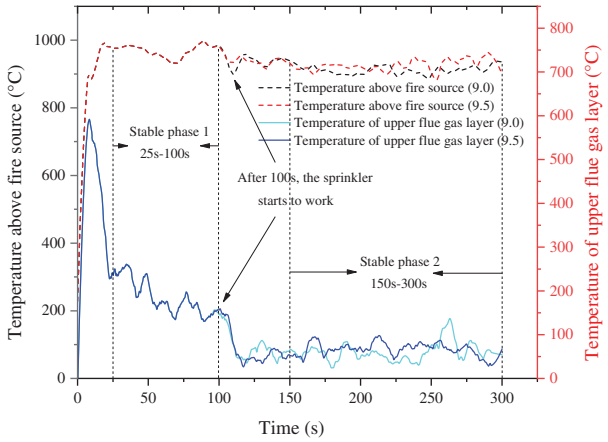

Figure 8: Temperature change curve above fire source at different sprinkler heights before and after the operation of the sprinkler

In Fig. 8, the solid line represents the temperature change curve of the upper flue gas layer. Interestingly, when the high-pressure water mist sprinkler is not working, the temperature profile of the upper flue gas layer stabilizes at approximately 25 s. Moreover, the average temperature of the upper flue gas layer (stable phase 1) is 186°C. After 100 s, the high-pressure water mist sprinkler starts, and the temperature of the upper flue gas layer decreases and finally stabilizes at about 125 s. In addition to this, for different sprinkler heights (9.0 and 9.5 m), the average temperature distributions of the upper flue gas layer (stable phase 2) are 60.8°C and 64°C. As a result, the conclusion can be drawn that for the same initial conditions, the lower sprinkler height has a good cooling effect on the upper flue gas layer.

As can be observed from Fig. 9, when the high-pressure water mist system is not working, the flue gas concentration reaches a stable state in about 25 s, whereas the average flue gas concentration change (stable phase 1) is 3.16×10^{-5} kg/m^3. Furthermore, after 100 s, the high-pressure water mist sprinkler begins to operate, the flue gas concentration decreases, and the flue gas concentration stabilizes at about 125 s. When the different sprinkler heights (9.0, 9.5 m) are also considered, the average flue gas concentration changes (stable phase 2) are 1.02×10^{-5} kg/m^3 and 1.29×10^{-5} kg/m^3.

Hence, it can be found that as the height of the high-pressure water mist sprinkler decreases, the flue gas concentration shows a decreasing trend.

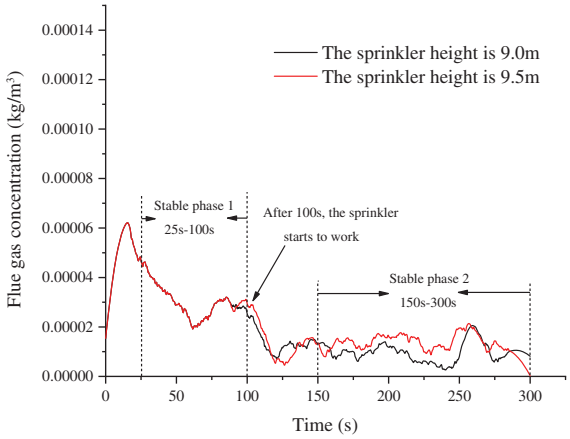

Figure 9: Change curve of the flue gas concentration above the fire source at different sprinkler heights before and after the operation of the sprinkler

3.3.2 Analysis of the Parameters of the Different Setting Schemes of the High-Pressure Water Mist

The dotted line in Fig. 10 represents the temperature change curve above the fire source. From the acquired outcomes, it can be observed that when the high-pressure water mist system is not working, the fire source reaches a stable state in approximately 25 s, while the average temperature change (stable phase 1) is 441°C. Subsequently, after 100 s, the high-pressure water mist sprinkler starts to work. As a result, the temperature above the fire source decreases and is stabilized at about 150 s. It should be emphasized that with the application of different layout strategies (sprinkler is not full or full), the average temperature changes above the fire source (stable phase 2) are 382°C and 326°C. It is thus obvious that for the same initial conditions, the high-pressure water mist sprinkler exhibits a good cooling effect when it is full.

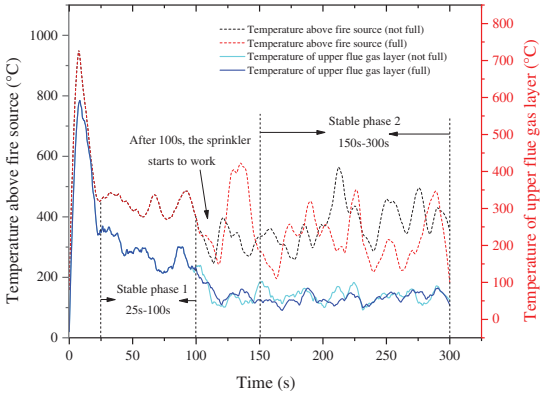

Figure 10: Temperature change curve above the fire source when employing different settings before and after the operation of the sprinkler

In Fig. 10, the solid line represents the temperature change curve of the upper flue gas layer. As can be ascertained from the figure, when the high-pressure water mist system is not working, the temperature distribution of the upper flue gas layer reaches a stable state in about 25 s, while the average temperature of the upper flue gas layer (stable phase 1) is 180°C. After 100 s, the high-pressure water mist sprinkler starts to work, and the temperature of the upper flue gas layer decreases and is stabilized at about 150 s. When different laying strategies are employed (sprinkler is not full or full), the average temperature values of the upper flue gas layer changes (stable phase 2) are 64.1°C and 56.5°C. Therefore, with the same initial conditions, when the high-pressure water mist sprinklers are full, they exhibit a good cooling effect on the temperature of the upper flue gas layer.

It is interesting to note that when the high-pressure water mist sprinkler is not working, the flue gas concentration reaches a stable state between 25 and 100 s, whereas the average calculated flue gas concentration change is 3.16×10^{-5} kg/m^3. After 100 s, the high-pressure water mist sprinkler begins to operate. As can be found in Table 3, the flue gas concentration above the transformer is reduced. Moreover, based on the average of the flue gas concentration changes after the sprinkler is started, the difference between the two cases is not large, while the two layouts have no obvious influence on the flue gas concentration.

Table 3: Average variation of the flue gas concentration

Sprinkler status	25–100 s	After 150 s
The sprinkler is not full	3.16×10^{-5} kg/m^3	1.39×10^{-5} kg/m^3
The sprinkler is full	3.16×10^{-5} kg/m^3	1.48×10^{-5} kg/m^3

4 Conclusions

To study the impact of a high-pressure water mist fire extinguishing system on transformer fires with the application of different external conditions, the FDS software is employed to model and analyze the extinguishing process of a high-pressure water mist system for transformer fires. The main conclusions of our work are as follows:

(1) From the point of view of the temperature changes at different heights on the centerline above the fire source, the farther away from the fire source the position is, the lower the local temperature distribution is.

(2) When a transformer fire event occurs at different ambient temperatures, the ambient temperature is lower and the viscosity of the fuel increases, which leads to a slower combustion rate of the droplet and a larger movement path for the droplet, which increases the length of the flame. The temperature above the fire source is relatively high. When the ambient temperature increases, the flame length decreases and the width increases, the chemical reaction activity of the combustion increases, the concentration of the flue gas decreases, the temperature above the fire source decreases as the flame height decreases. Therefore, in the range of relatively low ambient temperature, the temperature and smoke concentration above the fire source decrease to a certain extent as the ambient temperature increases.

(3) After the high-pressure water mist sprinkler is started, the temperature and the flue gas concentration above the fire source are both reduced, which demonstrates that the high-pressure water mist system has the ability to effectively cool down the temperature and

reduce the dust. Additionally, by comparing the different sprinkler layout methods, it is found that the low sprinkler height has a pronounced effect on the temperature above the fire source, the temperature of the upper flue gas layer, and the flue gas concentration. Furthermore, when the sprinkler is spread over the entire transformer, the sprinkler exhibits a good cooling effect on the temperature above the fire source and the temperature of the upper flue gas layer. Compared with the case when the sprinkler is not full, the change of flue gas concentration above the fire source is not obvious.

Funding Statement: This work was supported by Science and Technology Projects Funded by State Grid Corporation of China (5200202024105A0000).

Conflicts of Interest: The authors declare no conflict of interest.

References

1. Chen, B. H., Lu, J. Z., Liang, P., Sun, Y. C., Li, B. et al. (2019). Water mist enhanced extinguishing system and electrical transformer extinguishing test. *Fire Science and Technology, 38(1),* 107–110.
2. Gao, Z. X., Zhang, F., Gao, D., Zhang, J. G. (2019). Discussion on extinguishing scheme of UHVDC converter transformer. *Fire Science and Technology, 38(8),* 1106–1107+1116.
3. Li, J. T., Zhu, H. Y. (2012). Experiments on fire suppression of oil-filled transformer fire. *Fire Science and Technology, 31(12),* 1306–1309.
4. Chen, G., Jing, W., Wang, Z. G., Xu, L., Chen, P. (2019). Study on influence of fire source power on combustion characteristics of indoor transformer fire. *Journal of Safety Science and Technology, 15(7),* 186–192.
5. Chen, T., Wang, Y. W., Zhang, J. Q., Guo, Y. (2021). Study on the fire characteristics and smoke hazards of typical transformer oils. *Fire Science and Technology, 40(8),* 1125–1129.
6. Zhu, Z. G. (2017). Analysis of a transformer accident. *Metallurgical Industry Automation, 41(4),* 64–67.
7. Wang, H. F., Chen, C., Hu, L., Wang, X. J. (2018). Reflection and prevention of transformer fire typical case. *Distribution & Utilization, 35(11),* 78–82.
8. Chen, T., Zhao, L. Z., Fu, X. C., Zhang, J. Q., Wang, Q. et al. (2020). Fire accident characteristics and firefighting solutions of large converter transformer. *Fire Science and Technology, 39(8),* 1138–1141.
9. Wang, Y. L., Li, C. H., Zhang, J. Q., Sang, F. J., Lu, S. X. et al. (2019). Fire accident characteristics and fire extinguishing countermeasures of oil-immersed transformer. *Safety and Environmental Engineering, 26(6),* 166–171.
10. Sivrikaya, E., Iyigun, B., Tekin, M., Kivrak, M. F., Cavdar, E. et al. (2019). National legislation and international standards for fire detection and protection systems for industrial transformers and substations of industries facilities. *2019 6th International Conference on Electrical and Electronics Engineering (ICEEE)*, pp. 16–17. Istanbul, Turkey.
11. Fangrat, J., Kaczorek-Chrobak, K., Papis, B. K. (2020). Fire behavior of electrical installations in buildings. *Energies, 13(23),* 6433. DOI 10.3390/en13236433.
12. Lu, J. Z., Chen, B. H., Liang, P., Sun, Y. C., Fang, Z. et al. (2019). Experimental evaluation of protecting high-voltage electrical transformers using water mist with and without additives. *Fire Technology, 55(5),* 1671–1690. DOI 10.1007/s10694-019-00825-9.
13. Liu, Q. Y., Yi, X. Y., Lv, Z. H., Zhang, Z. (2019). Progress on water mist fire suppression effectiveness. *Science Technology and Engineering, 19(22),* 11–19.

14. Wang, M. W., Tao, B., Li, J. W., He, Y. H. (2020). Experimental study on the effectiveness and safety of water mist in electrical fire fighting. *Fire Science and Technology, 39(7),* 969–972.
15. Chen, B. Y., Yang, Y. B., Bing, Z., Shi, J., Wang, X. P. (2019). Study on the influence of fine water mist particle size on fire extinguishing effect of cable cabin in underground utility tunnel. *Fire Science and Technology, 38(6),* 832–836.
16. Chen, Q., Wei, X., Chen, G., Wang, Z. G., Li, G. J. et al. (2020). Research on the atomization characteristics of fine water under different pressure. *Fire Science and Technology, 39(6),* 803–806.
17. Yang, L. J., Fu, Q. F., Wang, X. D., Liao, S. J. (2009). Experimental of effect of water mist nozzle injection pressure on fire extinguishing. *Journal of Beijing University of Aeronautics and Astronautics, 35(3),* 361–365.
18. Ma, J. Y., Nie, B., An, Z. L., Chang, X. D., Chen, B. D. (2020). Experimental research on fire extinguishing by high pressure water mist with different injection strategies. *Urban Mass Transit, 23(2),* 137–140.
19. Chan, S. J., Chi, Y. L. (2021). Experimental investigation on spray characteristics of twin-fluid sprinkler for water mist and its heptane pool fire extinguishing performance. *Process Safety and Environmental Protection, 148(4),* 724–736. DOI 10.1016/j.psep.2021.01.037.
20. Gong, Y. J., Yi, Z. Y., Wang, Z. W., Zhang, Z. M. (2010). Experiment and analysis on the combined sprinkler head with water mist nozzle. *Journal of Combustion Science and Technology, 16(6),* 542–546.
21. Lu, J. Z., Liang, P., Chen, B. H., Wu, C. P., Zhou, T. N. (2020). Investigation of the fire-extinguishing performance of water mist with various additives on typical pool fires. *Combustion Science and Technology, 192(4),* 529–609. DOI 10.1080/00102202.2019.1584798.
22. Wang, H. M., Wang, S. Y., Wang, X. L. (2021). Fire dynamic simulation of complex high pressure fine water mist characteristic parameters. *Science Technology and Engineering, 21(22),* 9644–9650.
23. Chen, B. H., Deng, J., Sun, Y. C., Li, B., Fang, Z. et al. (2020). Study on electrical insulation performance of water mist for electrical transformer. *Fire Science and Technology, 39(1),* 67–69.
24. Zhang, J., Shu, N., He, J. Z., Huang, H. B. (2019). Influence of sprinkler arrangement on water mist fire extinguishing in utility tunnel. *Fire Science and Technology, 38(2),* 236–239.
25. Wang, J. (2020). Experimental study on spraying dust reduction of roadway coal dust by high-pressure water mist nozzle. *Safety and Environmental Engineering, 27(5),* 38–41, 48.
26. Sun, R. B., Yang, X., Wang, J. C., Chen, P., Wu, L. S. (2021). Experimental study on axial temperature profile of jet fire of oil-filled equipment in substation. *Processes, 9(8),* 1460. DOI 10.3390/pr9081460.
27. Yuan, Y. P., Wu, S. F., Shen, B. Y. (2021). A numerical simulation of the suppression of hydrogen jet fires on hydrogen fuel cell ships using a fine water mist. *International Journal of Hydrogen Energy, 46(2),* 13353–13364.
28. Cheng, H., Peng, M. J., Cheng, Y. M. (2018). The dimension splitting and improved complex variable element-free Galerkin method for 3-dimensional transient heat conduction problems. *International Journal for Numerical Methods in Engineering, 114(3),* 321–345. DOI 10.1002/nme.5745.
29. Cheng, H., Peng, M. J., Cheng, Y. M. (2017). A hybrid improved complex variable element-free Galerkin method for three-dimensional potential problems. *Engineering Analysis with Boundary Elements, 84(5),* 52–62. DOI 10.1016/j.enganabound.2017.08.001.
30. Wu, S. F., Yuan, Y. P. (2020). Simulation study on suppression and extinguishing of ship engine room fire based on FDS with fine water mist. *Shipbuilding of China, 61(4),* 170–187.
31. McGrattan, K., Hostikka, S., McDermott, R., Floyd, J., Weinschenk, G. et al. (2010). *Fire dynamics simulator (version 6) user's guide*, pp. 1019. Gaithersburg, Maryland; National Institute of Standards and Technology.
32. Wu, D., Wang, Y. Q., Luo, J. Y., Li, D. H., Chen, Y. B. (2021). Numerical simulation study on the effect of water mist on the fire extinguishment of the comprehensive pipeline gallery. *Journal of Southwest University of Science and Technology, 36(2),* 49–54.

33. Zhong, W., Sun, C. P., Ma, W. H., Gao, Z. H., Zhao, J. (2021). Comparison of smoke exhaust effect between ceiling and lateral mechanical smoke exhaust in tunnel. *Fire Science and Technology, 40(5),* 639–643.
34. Xie, K., Qiu, X. Q., Cui, Y. J., Wang, J. X. (2019). Experimental study on flame morphology of horizontal jet spray combustion at different ambient temperature. *Industrial Heating, 48(2),* 17–20. DOI 10.3969/j.issn.1002-1639.2019.02.005.
35. Liu, J. J., Qiu, X. Q., Tian, X. S., Wang, K. (2018). Numerical analysis of the flame structural characteristics of light oil burner under different environmental conditions. *Journal of Shandong University of Science and Technology (Natural Science), 37(2),* 80–87.